

# PROCEEDINGS OF SPIE

[SPIDigitalLibrary.org/conference-proceedings-of-spie](https://spiedigitallibrary.org/conference-proceedings-of-spie)

## Parallel acoustic delay lines for photoacoustic tomography

Murat Kaya Yapici, Chulhong Kim, Cheng-Chung Chang, Mansik Jeon, Zijian Guo, et al.

Murat Kaya Yapici, Chulhong Kim, Cheng-Chung Chang, Mansik Jeon, Zijian Guo, Xin Cai, Jun Zou, Lihong V. Wang, "Parallel acoustic delay lines for photoacoustic tomography," Proc. SPIE 8581, Photons Plus Ultrasound: Imaging and Sensing 2013, 85811C (4 March 2013); doi: 10.1117/12.2003289

**SPIE.**

Event: SPIE BiOS, 2013, San Francisco, California, United States

# Parallel acoustic delay lines for photoacoustic tomography

Murat Kaya Yapici<sup>\*a</sup>, Chulhong Kim<sup>b</sup>, Cheng-Chung Chang<sup>c</sup>, Mansik Jeon<sup>b</sup>, Zijian Guo<sup>d</sup>, Xin Cai<sup>d</sup>, Jun Zou<sup>c</sup>, and Lihong V. Wang<sup>d</sup>

<sup>a</sup>Department of Electrical and Computer Engineering, Khalifa University, 127788, Abu Dhabi, UAE;

<sup>b</sup>Department of Biomedical Engineering, University at Buffalo-SUNY, Buffalo, NY 14260 USA;

<sup>c</sup>Department of Electrical and Computer Engineering, Texas A&M University, College Station, TX 77843

USA; <sup>d</sup>Department of Biomedical Engineering, Washington University-St. Louis, St. Louis, MO 63130 USA

## ABSTRACT

Achieving real-time photoacoustic (PA) tomography typically requires massive ultrasound transducer arrays and data acquisition (DAQ) electronics to receive PA waves simultaneously. In this paper, we report the first demonstration of a photoacoustic tomography (PAT) system using optical fiber-based parallel acoustic delay lines (PADLs). By employing PADLs to introduce specific time delays, the PA signals (on the order of a few micro seconds) can be forced to arrive at the ultrasonic transducers at different times. As a result, time-delayed PA signals in multiple channels can be ultimately received and processed in a serial manner with a single-element transducer, followed by single-channel DAQ electronics. Our results show that an optically absorbing target in an optically scattering medium can be photoacoustically imaged using the newly developed PADL-based PAT system. Potentially, this approach could be adopted to significantly reduce the complexity and cost of ultrasonic array receiver systems.

**Keywords:** Photoacoustic tomography, acoustic delay line, ultrasound transducer array, real-time imaging.

## 1. INTRODUCTION

Photoacoustic tomography (PAT) has emerged as a hybrid biomedical imaging technique which combines strong endogenous and exogenous optical absorption contrast and high ultrasonic resolution in a single modality [1-3]. In PAT, a short-pulsed laser irradiates the biological tissue, and photoacoustic (PA) waves are generated via thermoelastic expansion. These PA waves propagate in the medium and are then detected by a single-element ultrasonic transducer or an ultrasonic transducer array. The amplitudes of the initial PA waves, the multiplication between local fluence and the optical absorption coefficients of targets, represent the optical absorption distribution of the tissue. Thus, PAT overcomes the fundamental limitations of pure optical imaging (shallow imaging depth for high resolution, or poor spatial resolution beyond the transport mean free path) and pure ultrasonic imaging (weak contrast and speckle artifacts) [4-9]. It is capable of high-resolution structural [10, 11], functional [11-14], and molecular imaging [15-20]. By scaling the ultrasonic frequency, the spatial resolution and imaging depth can be tailored for particular imaging applications.

There are two main types of PAT systems [21]. The first is photoacoustic microscopy (PAM), which utilizes direct point by point detection of 1D depth-resolved images and raster mechanical scanning to form a 3D image. The second type is photoacoustic computed tomography (PACT), which uses ultrasonic transducer arrays for parallel detection and reconstruction algorithms for real-time image generation [22-25]. PAM does not require the use of a mathematical algorithm to generate an image, but it requires raster scanning with a single-element focused transducer. Consequently, the imaging speed of PAM depends largely on the laser repetition rate and the speed of the mechanical scanning. By contrast, PACT can be implemented using an ultrasound array system; hence, the imaging speed is dramatically improved without raster mechanical scanning. For example, Gamelin *et al.* [23] used a full-ring ultrasonic transducer array consisting of 512 elements to collect 2D images at a frame rate of 0.9 Hz, with a 10-Hz laser pulse repetition rate. The data acquisition (DAQ) electronics were composed of 512 low-noise preamplifiers. With 8:1 multiplexing, eight laser pulses were required to capture a complete 512-element data set. In addition, linear ultrasound transducer arrays with either 48 or 128 elements have been used in PACT [23, 25].

\*murat.yapici@kustar.ac.ae, murat.yapici@gmail.com; phone: 971-2-5018344; fax: 971-2-4472442

Photons Plus Ultrasound: Imaging and Sensing 2013, edited by Alexander A. Oraevsky, Lihong V. Wang,  
Proc. of SPIE Vol. 8581, 85811C · © 2013 SPIE · CCC code: 1605-7422/13/\$18 · doi: 10.1117/12.2003289

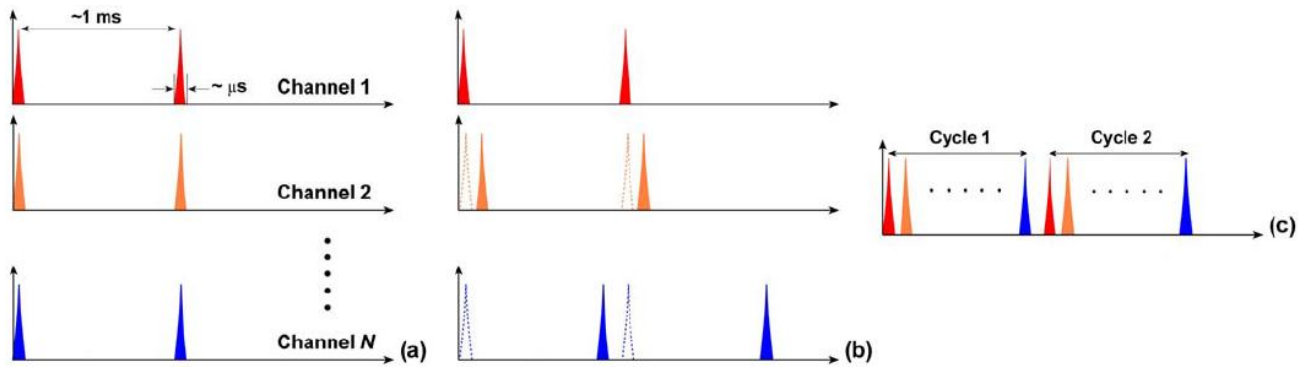


Figure 1. (a) PA signals without time delays (in current PACT systems); (b) PA signals with proper time delays; and (c) multiple channels of time-delayed PA signals mixed into one single channel.

Generally, the imaging speed of PACT depends on the number of transducer elements in the array. However, as the number of transducer elements increases, the construction and operation of the ultrasound receiving systems becomes more challenging and costly. Therefore, new solutions are needed to reduce or even completely eliminate the dependence on massive ultrasonic transducer arrays and extensive DAQ electronics.

Depending on the penetration depth (from a few mm to cm) and the acoustic velocity in the target tissue ( $\sim 1480$  m/s), the typical propagation time of a PA wave in the medium is on the order of microseconds ( $\mu\text{s}$ ) (Fig. 1a). On the other hand, the pulse repetition rate of the pulsed-laser systems used in PAT is in the kilohertz range, so the time interval between two successively generated PA waves will be on the order of milliseconds (ms). In current PACT systems, all the generated PA signals propagate and reach the ultrasonic transducers nearly simultaneously. This simultaneity inevitably leads to a parallel detection scheme, which requires multiple receiving channels (including ultrasonic transducers and DAQ electronics). However, by using parallel acoustic delay lines (PADLs) to introduce specific acoustic time delays (Fig. 1b), the PA signals in different channels can be forced to arrive at the ultrasonic transducers at different times, and will be completely distinguishable in the time domain even after being mixed into one channel (Fig. 1c). Ultimately, this technique opens the possibility of detecting and processing multiple channels of time-delayed PA signals in a serial manner, using a single-element transducer and single-channel DAQ electronics. Because the PA signals have a shorter propagation time ( $\mu\text{s}$ ) than the laser pulse repetition time (ms), this approach is potentially able to merge a large number of receiving channels, and thus leads to significant reductions in the complexity and cost of ultrasonic receiving systems.

In this paper, we report, for the first time to our knowledge, the development and application of a novel PADL technique for PAT. The PADLs are made of low-loss and flexible optical fibers. We experimentally characterized the acoustic properties of the optical fibers and verified the feasibility of using them as acoustic waveguides. Based on these results, the optical fibers were used to construct multi-channel PADLs where each channel independently carried PA waves with a specific time delay. We built a prototype PADL-PAT system using 16 optical-fiber PADLs, 2 ultrasound transducers, and 2 channels of DAQ electronics. The PADL-PAT system successfully imaged an optically absorbing object positioned in an optically scattering medium.

## 2. OPTICAL-FIBER ACOUSTIC WAVEGUIDES

Various materials, including liquid mercury [26], solid quartz crystals [27], metallic wires [28], and flexible optical fibers [29, 30], have been used to construct ultrasonic delay lines. Given the acoustic velocity in these media, we can control the acoustic time delay from  $\mu\text{s}$  to ms by varying the propagation length of the material without causing excessive acoustic attenuation [31]. To construct the delay line for this work, we selected optical fibers due their broad availability, low-cost, and low acoustic attenuation.

### 2.1 Propagation Modes in Optical Fibers

PA signals propagate in longitudinal modes. However, for wire-type cylindrical acoustic delay lines, all of the sustained longitudinal modes are dispersive, which means that the time delay is dependent on the frequency of the transmitted signal. This dispersion can generate signal distortion in the time domain, which is not desirable for PAT since the time-of-arrival of the PA signals is used to retrieve spatial information for image reconstruction. To address this

issue, the lowest-order longitudinal mode ( $L(0,1)$ ) of the Pochhammer-Chree wave was used. It has been shown that if the diameter of the circular fiber ( $d$ ) is much smaller than the ultrasound wavelength ( $\lambda$ ) both the higher-order longitudinal modes and the dispersion of the  $L(0,1)$  mode will be significantly suppressed. Typically, this condition is satisfied when  $(d/\lambda)$  or  $(df/V_0) < 0.1$ , where  $f$  is the frequency of the ultrasonic wave, and  $V_0$  is the acoustic velocity in a rod [28, 32]. A smaller ratio of  $(df/V_0)$  would further suppress higher order modes and the dispersion of the  $L(0,1)$  mode. Thus, once  $d$  is small enough that the above inequality is satisfied for all detected wave components, high-fidelity transmission of the PA signal through the acoustic delay lines can be achieved. For PA signal detection at a 1 MHz center frequency, and based on previously reported acoustic velocity data for optical fibers (5000-6000 m/s) [32, 33], fused-silica optical fibers (CeramOptec Inc., MA) with a total diameter of  $\sim 245 \mu\text{m}$  (including core, cladding and jacket) were selected, which provided  $(df/V_0) < 0.05$ .

## 2.2 Characterization Method

To build an optical fiber-based delay line, the acoustic properties (i.e., attenuation, propagation velocity, and time delay) of fused-silica optical fibers were characterized. The schematic and a photograph of the experimental setup are shown in Fig. 2. The optical fiber was loosely mounted onto a phenolic-based (acrylic) perforated board (proto-board). The perforated board provided good acoustic isolation due to the large acoustic impedance mismatch between the board (acrylic) and the fiber (silica). In addition, unnecessary contact between the fiber and surrounding structures was minimized to reduce acoustic reverberation. Two identical flat, longitudinal mode PZT ultrasound transducers with a center frequency of 1 MHz (Olympus NDT, V303) were used. The fiber tips were polished and carefully coupled to the transducer surface via a thin layer of ultrasound gel. This coupling also helped to filter out the unwanted shear, torsional, and extensional modes of the ultrasonic waves. Optical fibers with various lengths were tested for acoustic attenuation, ultrasound propagation speed, and time delay. As shown in Fig. 2b, an ultrasound pulse (1  $\mu\text{s}$  width and 500 mV<sub>pp</sub> amplitude) was generated by a signal generator, amplified by an RF amplifier, and applied to the transmitting transducer. Ultrasound pulses from the transmitting transducer propagated through the optical fiber and were detected by the receiving transducer. The received signals were amplified and displayed on an oscilloscope.

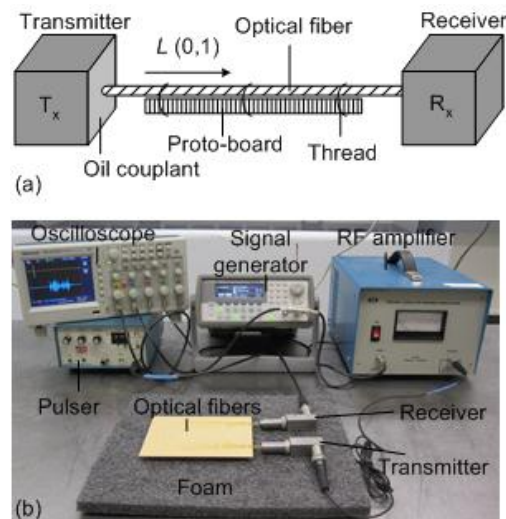


Figure 2. (a) Schematic showing the arrangement of transducers with respect to the optical fiber under characterization; and (b) photograph of the entire experimental setup for acoustic characterization of optical fibers.

## 2.3 Acoustic Properties: Attenuation, velocity, and time delay

Fig. 3a shows the detected ultrasound waveforms of the six optical fibers as well as the ultrasound pulse applied to the transmitting transducer. Distinct signals at an incremental time delay of  $\sim 10 \mu\text{s}$  were received for fibers of lengths ranging from 10 cm to 35 cm. For shorter fibers, the 1<sup>st</sup> echo signals resulting from acoustic reflection between the fiber and the surface of the receiving transducer are also displayed. The echoes were detected at a time corresponding to three traversals of the fiber length. The time delay of each fiber is plotted in Fig. 3b. As the fiber length increases, the time delay increases linearly. Based on these measurements, the average acoustic velocity in fused-silica optical fiber was found to be  $\sim 5108 \text{ m/s}$ .

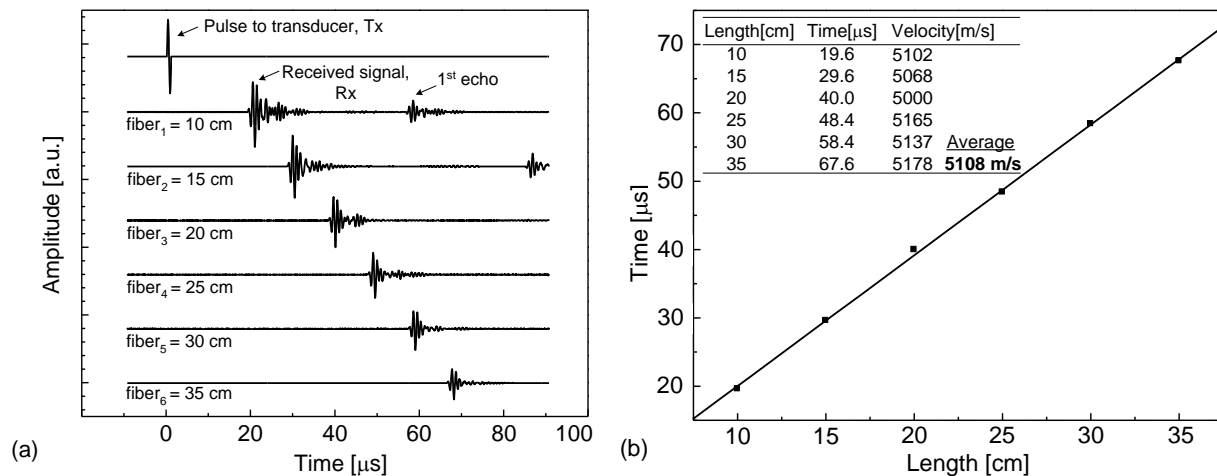


Figure 3. (a) Plot showing acoustic waveforms propagating through optical fibers of different lengths ranging from 10 cm to 35 cm. (b) Plot of the time delay versus the corresponding fiber length. The average acoustic velocity in the fused-silica fiber is ~ 5108 m/s.

To determine the acoustic attenuation in the optical fibers, the amplitudes of the received ultrasound waves are also plotted (Fig. 4). The acoustic loss ( $L$ ) is defined by  $20\log(V_{out}/V_{in})$ , where  $V_{in}$  refers to the acoustic signal amplitude at the fiber input, and  $V_{out}$  refers to the amplitude at the output. The acoustic attenuation constant can be calculated by dividing the acoustic loss by the length of the optical fiber. However, it is difficult to directly measure  $V_{in}$ . Therefore, losses of two different fibers having a certain length difference ( $\Delta l$ ) were subtracted. Then, the loss over  $\Delta l$  length is  $20\log(V_{out,i}/V_{out,1})$ , where  $V_{out,1}$  (the shorter fiber) was kept constant in all calculations, and  $V_{out,i}$  corresponds to the output amplitudes of the remaining five fibers ( $i=2$  to  $i=6$ ). Based on this approach, five data points for loss (i.e.,  $L_{2,1}$  to  $L_{6,1}$ ) were obtained (inset in Fig. 4), and the average attenuation per unit length or unit time delay was calculated as ~ 0.2 dB/cm (i.e., 0.1 dB/μs) at 1 MHz, which matches well with previously reported data [32].

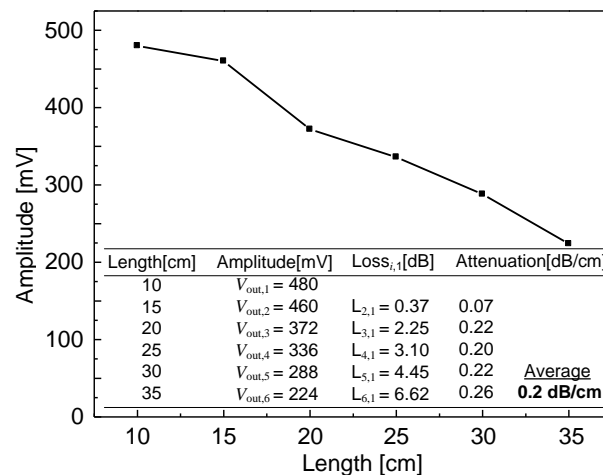


Figure 4. Plot of the received acoustic signal amplitude versus optical fiber length; average attenuation is ~ 0.2 dB/cm (0.1 dB/μs).

To analyze the frequency responses of the optical fibers, fast Fourier transform (FFT) was performed on their time-domain responses (ultrasound waveforms in Fig. 3a) using the built-in FFT algorithm of MATLAB®. Power spectra of the six different optical fibers are plotted on the same chart for comparison (Fig. 5). On average, the signals have a center frequency ( $f_o$ ) at ~ 1 MHz and -6dB bandwidth of ~ 0.5 MHz, with upper and lower frequency cutoffs at ~0.85 MHz and ~1.35 MHz, respectively. The received power spectra of the fibers are in good agreement with the frequency specifications ( $f_o \sim 1$  MHz) of the transmitting transducer [34].

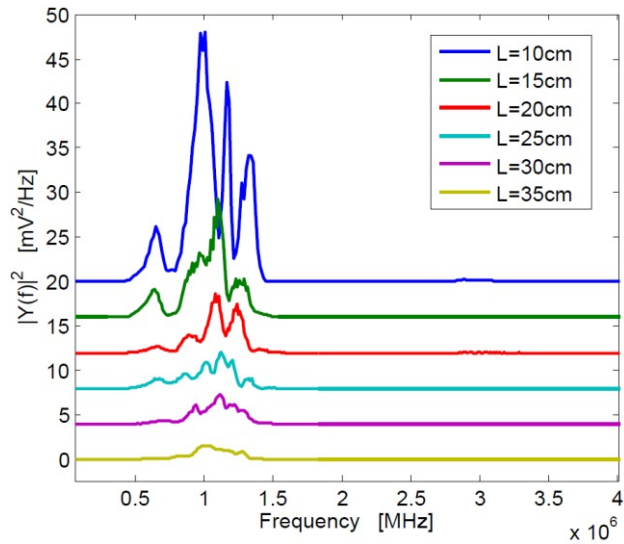


Figure 5. Frequency responses (power spectra) of the six optical fibers with different lengths, showing a center frequency of  $\sim 1$  MHz.

### 3. PARALLEL ACOUSTIC DELAY LINES (PADLS)

The optical-fiber PADLs were designed based on the measured acoustic properties of optical fibers. The following design parameters were also considered: (1) the number of fibers (i.e., the number of delay lines,  $n$ ), (2) the length of each fiber determining the time delay, and (3) the parallel arrangement of fibers and the pitch between fibers. As  $n$  increases, the construction and handling of the PADLs becomes difficult due to the longer fiber lengths. In this work,  $n$  was selected as 8 to ensure a compact design and an adequate field-of-view (FOV), which is also related to the fiber diameter, pitch, and target size in PA imaging. When the fiber lengths were determined, the following two design criteria were considered. First, the time delay between each fiber (i.e., channel spacing) should be long enough to prevent possible signal overlaps from adjacent channels. Based on the duration ( $\sim 12 \mu\text{s}$ ) of the ultrasonic signals arriving at the receiving transducer, an incremental time delay ( $\geq 12 \mu\text{s}$ ) between adjacent delay lines is required to avoid signal overlapping. The second criterion concerning fiber lengths is to select the proper arrival time for reflected signals (1<sup>st</sup> echo) in the shortest fiber (1<sup>st</sup> fiber). To prevent possible interference between echoes and the original signals propagating in neighboring fibers, the fiber with the longest time-delay ( $n^{\text{th}}$  fiber) should be designed so that its signal reaches the receiving transducer before the 1<sup>st</sup> fiber's echo does. Denoting  $T$  as the incremental time delay between two neighboring fibers, and  $T_1$  as the time delay of the 1<sup>st</sup> fiber, the signal in the  $n^{\text{th}}$  fiber will be received at  $T_1 + T(n-1)$ , while the 1<sup>st</sup> fiber's echo will be received at  $3T_1$ . Then, to prevent interference, the following inequality must hold:  $3T_1 > T_1 + T(n-1)$ . Therefore, for an 8-fiber delay line and 12- $\mu\text{s}$  incremental time delay,  $T_1$  should be longer than 42  $\mu\text{s}$ . Based on this result, the 1<sup>st</sup> and 8<sup>th</sup> fibers were designed to provide time delays of 44  $\mu\text{s}$  and 224  $\mu\text{s}$ , respectively, which creates a 4- $\mu\text{s}$  gap between the arrival of the 1<sup>st</sup> fiber's echo and the signal in the 8<sup>th</sup> fiber. Table 1 summarizes the time delays for the 8-channel optical-fiber PADLs, along with the corresponding fiber lengths.

Table 1. Time Delays and Fiber Lengths for PADLs

Fiber Number	Time Delay [ $\mu\text{s}$ ]	Optical Fiber Length [mm]
1	44	225
2	56	286
3	68	347
4	80	409
5	92	470
6	104	531
7	116	593
8	128	654

The incremental time delay between fibers is 12  $\mu\text{s}$ , and the acoustic velocity in fused-silica optical fibers is  $\sim 5108$  m/s.

In ultrasound array systems, it is common to arrange the transducer elements with  $p < \lambda/2$ , where  $p$  is the pitch and  $\lambda$  is the wavelength. Based on the ultrasound frequency (1 MHz) of our ultrasound transducers, the fiber-to-fiber spacing would be in the range of 400-500  $\mu\text{m}$ . To arrange the optical-fiber PADLs, evenly-spaced  $\sim 200 \mu\text{m}$  wide trenches were made in a low-loss acoustic material (lucite) (Fig. 6a). The fibers were loosely placed in the trenches, which allowed the fibers to be arranged side-by-side in parallel, with the correct pitch and minimal attenuation. A total of sixteen fibers are housed in a common input port for PA signal detection, and separated into two output ports for time-delayed read-out (Fig. 6b). The selected geometrical dimensions, including the fiber diameter and spacing, as well as the number of fibers provide an effective FOV of  $\sim 1 \text{ cm}$ .

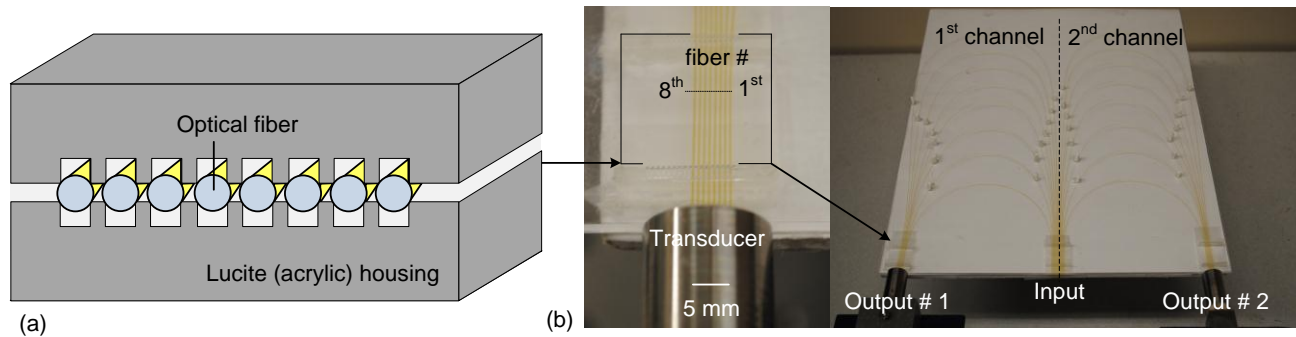


Figure 6. (a) Schematic of the parallel-fiber arrangement in equally-spaced trenches. (b) Pictures of the acrylic housing and the PADL array having a common input and two output channels.

## 4. PHOTOACOUSTIC IMAGING WITH PADLS

### 4.1 Photoacoustic imaging experiment

Fig. 7 shows the PA experimental setup. The light was delivered from a tunable OPO laser (Surelite OPO PLUS; Continuum; with a wavelength tunability of 410 nm to 2500 nm) pumped by a Q-switched Nd:YAG laser (SLII-10; Continuum) with a 5-nanosecond pulse duration and a 10-Hz pulse repetition rate. A light wavelength of 800 nm was used. The cylindrically focused light beam, horizontally parallel to the PADLs, illuminated the sample. This dark-field light illumination helped reduce the generation of unwanted surface signals and improved the signal-to-noise ratio (SNR). The incident laser pulse energy was less than  $5 \text{ mJ/cm}^2$ , far below the ANSI safety limit of  $31 \text{ mJ/cm}^2$  at this wavelength.

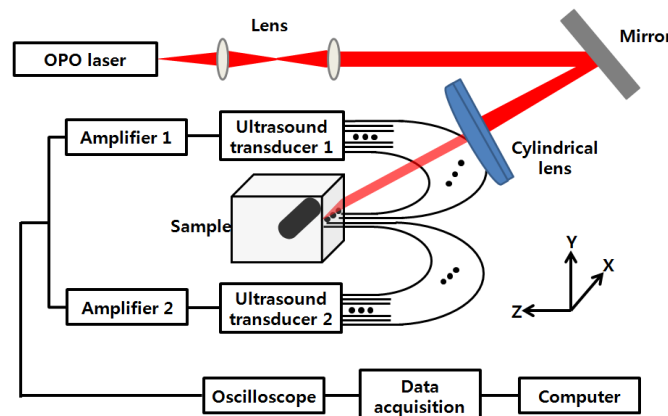


Figure 7. PA experimental setup using 16 channels of optical-fiber PADLs with two DAQ channels. Each DAQ channel interfaces with 8 optical-fiber PADLs.

Generated PA waves were detected by the PADLs, which were divided into two channels. For each channel, eight distinct PA waves propagating via the optical fibers were time-delayed and serially detected by a single-element unfocused ultrasound transducer with a center frequency of 1 MHz (Olympus NDT, V303). The PA signals were amplified and received by an oscilloscope. To enhance the coupling efficiency and minimize unwanted ultrasound

reverberation, ultrasound gel was applied at the interfaces between the optical fibers and the ultrasound transducer surface. A standard PAT reconstruction algorithm was employed to reconstruct the PA image, and the Hilbert transformation was taken in the axial direction for envelope detection [35].

#### 4.2 Photoacoustic image

To investigate the potential for cross-sectional imaging, an optically scattering tissue phantom ( $100 \text{ mm} \times 100 \text{ mm} \times 50 \text{ mm}$  along the X, Y, and Z axes, respectively) containing an optically absorptive object ( $5 \text{ mm} \times 2 \text{ mm} \times 2 \text{ mm}$  along the X, Y, and Z axes, respectively) was used (Fig. 8a). The target was positioned at a depth of 3 mm from the sample surface. The phantom was made of 10% gelatin by weight and 1% intra-lipid by volume, and its reduced scattering coefficient was  $\sim 9 \text{ cm}^{-1}$ . The A-scan PA signals received from the two channels are shown in Figs. 8b and 8c. Each A-scan sequentially recorded PA signals detected by each fiber. In theory, the PA signals from each fiber can be distinguished by calculating the fiber length differences and the acoustic velocity in the fiber. However, even minor measurement errors of these two parameters may cause inaccurate time delays and severely distort the image reconstruction. To address this issue, the starting points of the fibers were directly measured by painting the fiber tips with black ink, which also generated PA signals upon laser illumination. Thus the peaks of the PA signals from the ink on the fiber tips can be treated as the starting points and help indicate the actual PA signals corresponding to the imaged target.

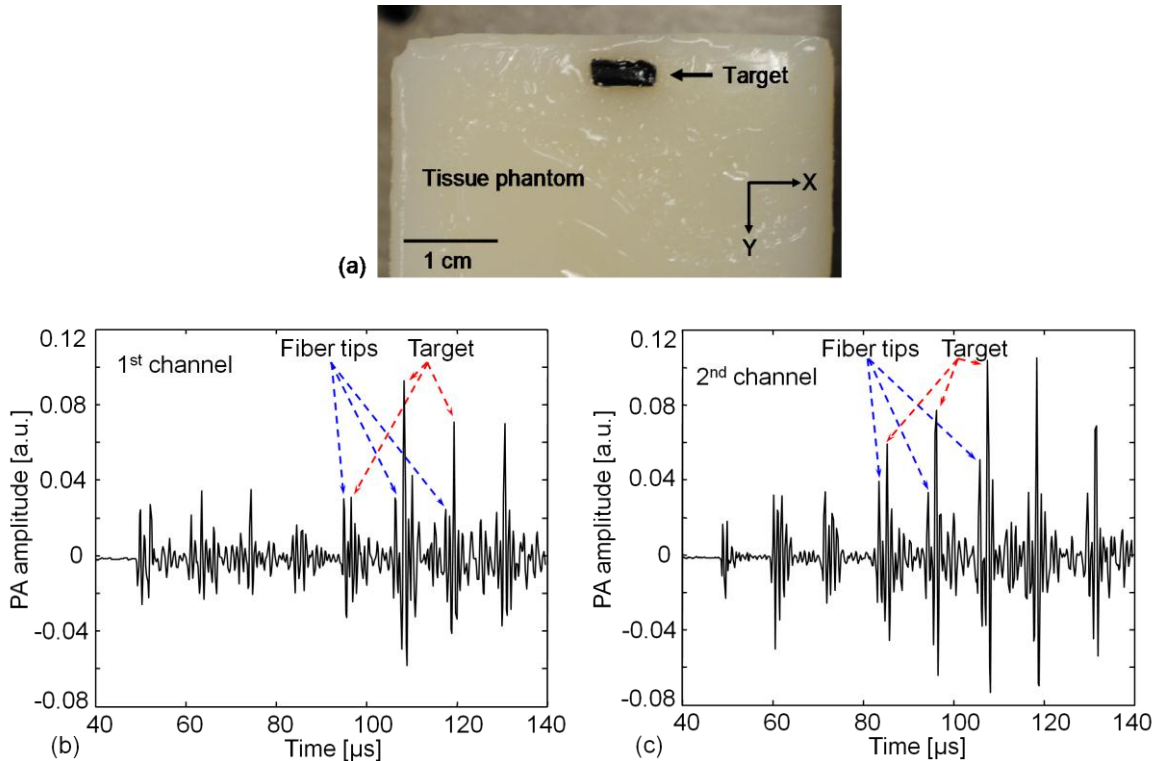


Figure 8. Reconstructed PA image of an optically absorptive target embedded in an optically scattering medium. (a) Photograph. (b) Raw A-scan data received by the 1<sup>st</sup> channel. (c) Raw A-scan data received by the 2<sup>nd</sup> channel.

The PA signals were averaged 100 times, so the imaging speed for one PA image was 10 seconds. A-scans from both ultrasonic transducers were reshaped and combined into one data set, as shown in Fig. 9a. The reconstructed PA image is shown in Fig. 9b, which matches well with the photograph in Fig. 8a. The image contrast is estimated to be  $\sim 2.3$ . The spatial resolution, defined as the one-way distance across the 10% and 90% points between the maximum and minimum of the edge spread function, is  $\sim 800 \mu\text{m}$ .

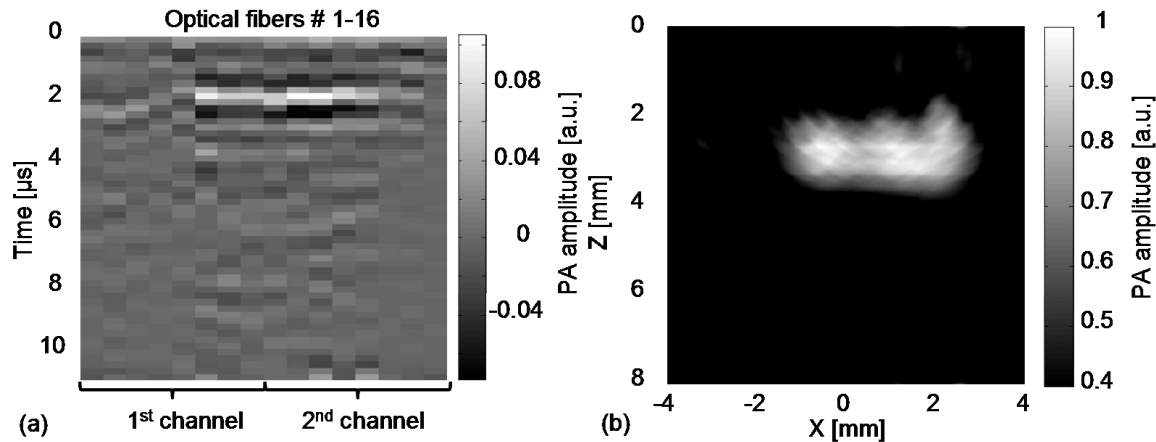


Figure 9. (a) Reshaped raw data acquired by both channels. (b) Reconstructed PA image.

## 5. CONCLUSION

In this work, we have developed parallel-acoustic-delay-line (PADL)-based photoacoustic tomography (PAT), where multiple channels of PA signals are time-delayed to reduce the complexity of the ultrasonic receiving systems. To provide the needed time-delay, the performance of fused-silica optical fibers serving as acoustic waveguides was experimentally characterized and a 16-channel PADL array was constructed. The functionality of PADL-PAT was demonstrated by conducting PA imaging of a tissue phantom housing an optically absorptive object. By using the PADLs, only two transducers and two channels of DAQ electronics were needed for the PA imaging. In contrast, a conventional PACT would require a 16-element ultrasonic transducer array and 16 channels of DAQ electronics. In this case, ~90% hardware reduction was achieved with the PADL approach. Once fully developed and optimized, the PADL approach could be applied to enhance the clinical applications of real-time 2-D or even 3-D photoacoustic and ultrasound imaging with significantly reduced system cost.

## REFERENCES

- [1] A. A. Oraevsky and A. A. Karabutov, in *Biomedical Photonics Handbook* Vol. PM125 (ed T. Vo-Dinh), CRC Press, 2003, ch. 34., pp. 3401-3434.
- [2] C. Kim, C. Favazza, and L. V. Wang, "In vivo photoacoustic tomography of chemicals: high-resolution functional and molecular optical imaging at new depths," *Chem. Rev.*, vol. 110, pp. 2756-2782, May. 2010.
- [3] L.V. Wang, *Photoacoustic Imaging and Spectroscopy*. CRC Press, 2009.
- [4] M.-L. Li, J.-T. Oh X.-Y. Xie, G. Ku, W. Wang, C. Li, G. Lungu, G. Stoica, and L. V. Wang, "Simultaneous molecular and hypoxia imaging of brain tumors in vivo using spectroscopic photoacoustic tomography," *Proc. of the IEEE*, vol. 96, pp. 481-489, Feb. 2008.
- [5] T. Wilson and C. Sheppard, *Theory and Practice of Scanning Optical Microscopy*. London: Academic Press, 1984.
- [6] D. A. Sipkins, X. B. Wei, J. W. Wu, J. M. Runnels, D. Cote, T. K. Means, A. D. Luster, D. T. Scadden, and C. P. Lin, "In vivo imaging of specialized bone marrow endothelial microdomains for tumour engraftment," *Nature*, vol. 435, pp. 969- 973, Jun. 2005.
- [7] W. Denk, J. H. Strickler, and W. W. Webb, "Two-photon laser scanning fluorescence microscopy," *Science*, vol. 248, pp. 73, Apr. 1990.
- [8] P. T. C. So, C. Y. Dong, B. R. Masters, and K. M. Berland, "Two-photon excitation fluorescence microscopy," *Ann. Rev. Biomed. Eng.*, vol. 2, pp. 399-429, Aug. 2000.
- [9] Z. Guo, L. Li, and L. V. Wang, "On the speckle-free nature of photoacoustic tomography," *Med. Phys.*, vol. 36, pp. 4084-4088, Sep. 2009.
- [10] H. F. Zhang, K. Maslov, G. Stoica, and L. V. Wang, "Functional photoacoustic microscopy for high-resolution and noninvasive in vivo imaging," *Nat. Biotechnol.*, vol. 24, 848-851, Jun. 2006.

- [11] X. Wang, Y. Pang, G. Ku, X. Xie, G. Stoica, and L. V. Wang, "Non-invasive laser-induced photoacoustic tomography for structural and functional imaging of the brain in vivo," *Nat. Biotechnol.*, vol. 21, pp. 803–806, Jun. 2003.
- [12] R. I. Siphanto, K. K. Thumma, R. G. M. Kolkman, T. G. van Leeuwen, F. F. M. de Mul, J. W. van Neck, L. N. A. van Adrichem, and W. Steenbergen, "Serial noninvasive photoacoustic imaging of neovascularization in tumor angiogenesis," *Opt. Express*, vol. 13, pp. 89-95, Jan. 2005.
- [13] J. Laufer, D. Delpy, C. Elwell, and P. Beard, "Quantitative spatially resolved measurement of tissue chromophore concentrations using photoacoustic spectroscopy: application to the measurement of blood oxygenation and hemoglobin concentration," *Phys. Med. Biol.*, vol. 52, pp. 141-168, Jan. 2007.
- [14] S. Yang, D. Xing, Q. Zhou, L. Xiang, and Y. Y. Lao, "Functional imaging of cerebrovascular activities in small animals using high-resolution photoacoustic tomography," *Med. Phys.*, vol. 34, pp. 3294-3301, Aug. 2007.
- [15] L. Li, R. J. Zemp, G. Lungu, G. Stoica, and L. V. Wang, "Photoacoustic imaging of lacZ gene expression in vivo," *J. Biomed. Opt.*, vol. 12, pp. 020504, Apr. 2007.
- [16] A. De La Zerda1, C. Zavaleta, S. Keren, S. Vaithilingam, S. Bodapati1, Z. Liu, J. Levi, B. R. Smith, T. Ma, O. Oralkan, Z. Cheng, X.-Y. Chen, H.-J. Dai, B. T. Khuri-Yakub, and S. S. Gambhir, "Carbon nanotubes as photoacoustic molecular imaging agents in living mice," *Nat. Nanotechnol.*, vol. 3, pp. 557-562, Sep. 2008.
- [17] John A. Copland, M. Eghtedari, V. L. Popov, N. Kotov, N. Mamedova, M. Motamedi, and A. A. Oraevsky, "Bioconjugated gold nanoparticles as a molecular based contrast agent: Implications for imaging of deep tumors using optoacoustic tomography," *Mol. Imaging Biol.*, vol. 6, pp. 341-349, Oct. 2004.
- [18] S. Mallidi, T. Larson, J. Aaron, K. Sokolov, and S. Emelianov, "Molecular specific optoacoustic imaging with plasmonic nanoparticles," *Opt. Express*, vol. 15, pp. 6583-6588, May. 2007.
- [19] D. Razansky and V. Ntziachristos, "Hybrid photoacoustic fluorescence molecular tomography using finite element-based inversion," *Med. Phys.*, vol. 34, pp. 4293-4301, Nov. 2007.
- [20] C. Kim, E. C. Cho, J. Chen, K. H. Song, L. Au, C. Favazza, Q. Zhang, C. M. Cobley, F. Gao, Y. Xia, and L. V. Wang, "In vivo molecular photoacoustic tomography of melanomas targeted by bio-conjugated gold nanocages," *ACS Nano*, vol. 4, pp. 4559-4564, Jul. 2010.
- [21] L. V. Wang, "Multiscale photoacoustic microscopy and computed tomography," *Nat. Photon.*, vol. 9, pp. 503-509, Sep. 2009.
- [22] M. P. Fronheiser, S. A. Ermilov, H. P. Brecht, A. Conjusteau, R. Su, K. Mehta, and A. A. Oraevsky, "Real-time optoacoustic monitoring and three-dimensional mapping of a human arm vasculature," *J. Biomed. Opt.*, vol. 15, pp. 021305, Apr. 2010.
- [23] J. Gamelin, A. Maurudis, A. Aguirre, F. Huang, P. Guo, L. V. Wang, and Q. Zhu, "A real-time photoacoustic tomography system for small animals," *Opt. Express*, vol. 17, pp. 10489-10498, Jun. 2009.
- [24] L. Song, C. Kim, K. Maslov, K. Song, and L. V. Wang, "High-speed dynamic 3-D photoacoustic imaging of sentinel lymph node in a murine model using an ultrasound array," *Med. Phys.*, vol. 361, pp. 3724-3729, Aug. 2009.
- [25] C. Kim, E. Todd, K. Maslov, L. Jankovic, W. J. Arkers, S. Achilefus, J. Margenthaler, M. Pashley, and L. V. Wang, "Handheld array-based photoacoustic probe for guiding needle biopsy of sentinel lymph nodes," *J. Biomed. Opt.*, vol. 15, pp. 046010, Aug. 2010.
- [26] I. L. Auerbach, J. P. Eckert, R. F. Shawt, and C. B. Sheppard, "Mercury delay line memory using a pulse rate of several megacycles," *Proc. of the IRE*, vol. 37, pp. 855-861, Aug. 1949.
- [27] D. L. Arenberg, "Ultrasonic solid delay lines," *J. Acoustic Soc. America*, vol. 20, pp. 1-26, Jan. 1948.
- [28] J. E. May, "Wire-type dispersive ultrasonic delay lines," *IRE Trans. Ultrason. Eng.*, vol. 7, pp. 44-52, Jun. 1960.
- [29] G. D. Boyd, L. A. Coldren, and R. N. Thurston, "Acoustic clad fiber delay lines," *IEEE Trans. Son. Ultrason.*, vol. su-24, pp. 246-252, Jul. 1977.
- [30] T. Moriya, Z. Hu, and Y. Tanahashi, "Development of flexible acoustic transmission line for intravascular ultrasonography," *IEEE Ultrason. Symp.*, Puerto Rico, 2000, pp. 1227-1230.
- [31] J. S. Palfreeman, "Acoustic delay lines-a survey of types and uses," *Ultrasonics*, vol. 3, pp. 1-8, Jan.-Mar. 1965.
- [32] I. L. Gelles, "Optical fiber ultrasonic delay lines," *J. Acoustic Soc. America*, vol. 39, pp. 1111-1119, Jan. 1966.
- [33] E. A. Lindgren, M. Rosen, and Kamal E. Amin, "Ultrasonic characterization of ceramic fibres at ambient and elevated temperatures," *Ultrasonics*, vol. 32, pp. 411-419, Jun. 1994.
- [34] *Panametrics Ultrasonic Transducers Data Sheet*, Olympus NDT, Massachusetts, 2006.
- [35] M. Xu and L. V. Wang, "Universal back-projection algorithm for photoacoustic-computed tomography," *Phys. Rev. E*, vol. 71, pp. 016706, Jan. 2005.